Assessing the Impact of Soil Layer Depth Specification on the Observability of Modeled Soil Moisture and Brightness Temperature

PETER J. SHELLITO,[a,b] SUJAY V. KUMAR,[b] JOSEPH A. SANTANELLO JR.,[b] PATRICIA LAWSTON-PARKER,[a,b] JOHN D. BOLTEN,[b] MICHAEL H. COSH,[c] DAVID D. BOSCH,[d] CHANDRA D. HOLIFIELD COLLINS,[e] STAN LIVINGSTON,[f] JOHN PRUEGER,[g] MARK SEYFRIED,[h] AND PATRICK J. STARKS[i]

[a] *Earth System Science Interdisciplinary Center, University of Maryland, College Park, College Park, Maryland*
[b] *Hydrological Sciences Laboratory, NASA GSFC, Greenbelt, Maryland*
[c] *Hydrology and Remote Sensing Laboratory, Agricultural Research Service, USDA, Beltsville, Maryland*
[d] *Southeast Watershed Research Laboratory, Agricultural Research Service, USDA, Tifton, Georgia*
[e] *Southwest Watershed Research Center, Agricultural Research Service, USDA, Tucson, Arizona*
[f] *National Soil Erosion Laboratory, Agricultural Research Service, USDA, West Lafayette, Indiana*
[g] *National Laboratory for Agriculture and Environment, Agricultural Research Service, USDA, Ames, Iowa*
[h] *Northwest Watershed Research Laboratory, Agricultural Research Service, USDA, Boise, Idaho*
[i] *Grazinglands Research Laboratory, Agricultural Research Service, USDA, El Reno, Oklahoma*

(Manuscript received 7 December 2019, in final form 14 July 2020)

ABSTRACT

The utility of hydrologic land surface models (LSMs) can be enhanced by using information from observational platforms, but mismatches between the two are common. This study assesses the degree to which model agreement with observations is affected by two mechanisms in particular: 1) physical incongruities between the support volumes being characterized and 2) inadequate or inconsistent parameterizations of physical processes. The Noah and Noah-MP LSMs by default characterize surface soil moisture (SSM) in the top 10 cm of the soil column. This depth is notably different from the 5-cm (or less) sensing depth of L-band radiometers such as NASA's Soil Moisture Active Passive (SMAP) satellite mission. These depth inconsistencies are examined by using thinner model layers in the Noah and Noah-MP LSMs and comparing resultant simulations to in situ and SMAP soil moisture. In addition, a forward radiative transfer model (RTM) is used to facilitate direct comparisons of LSM-based and SMAP-based L-band Tb retrievals. Agreement between models and observations is quantified using Kolmogorov–Smirnov distance values, calculated from empirical cumulative distribution functions of SSM and Tb time series. Results show that agreement of SSM and Tb with observations depends primarily on systematic biases, and the sign of those biases depends on the particular subspace being analyzed (SSM or Tb). This study concludes that the role of increased soil layer discretization on simulated soil moisture and Tb is secondary to the influence of component parameterizations, the effects of which dominate systematic differences with observations.

1. Introduction

Land surface models (LSMs) are important tools for understanding the cycle of water and energy between the land and the atmosphere. Because of the spatially limited and discontinuous nature of land surface observations, numerical schemes that constitute LSMs are necessary to fill information gaps in both space and time. The quantity of moisture contained within the soil is central to these simulations. Soil moisture affects infiltration and discharge rates and controls how net radiation is partitioned between sensible and latent heating. These fluxes, in turn, affect transpiration rates, the carbon cycle, weather and climate forecasts, and drought and flood assessments, all of which have humanitarian and environmental impacts.

One way to enhance the utility of a hydrologic LSM is to pass it observational information through data

Supplemental information related to this paper is available at the Journals Online website: https://doi.org/10.1175/JHM-D-19-0280.s1.

Corresponding author: Peter J. Shellito, shellito@gmail.com

DOI: 10.1175/JHM-D-19-0280.1

assimilation (DA) using a formal framework such as the ensemble Kalman filter (EnKF; Kumar et al. 2014a; Reichle et al. 2002). At the simplest level, DA involves updating simulated values toward those from an observation-based platform or network. Natural or anthropogenic processes that are present in observations but not explicitly accommodated by a model (or passed into a model via forcing data) can be at least partially captured through DA, resulting in improved outcomes for regional and global models (e.g., Felfelani et al. 2018; Rains et al. 2017; De Lannoy and Reichle 2016a,b). Datasets from remotely sensed observations are particularly attractive for DA because of their large-scale and distributed nature (Lahoz and De Lannoy 2014). Standard DA methods work optimally when the errors between the LSM and observations are random (Kumar et al. 2012b). As a result, DA frameworks require careful consideration of the nature of systematic errors (Crow et al. 2019). In the ideal scenario, observations would provide unbiased characterizations of the world, and models would be developed to provide unbiased estimates of those observations. Model-simulated values and corresponding observations would agree. Working toward this goal of model ''observability'' requires internal consistency in modeling systems. [For example, a model may provide accurate evapotranspiration estimates but if the soil moisture state required to achieve this end is not realistic and does not agree with the available soil moisture observations, then the model is inherently limited in its applicability (Koster et al. 2009).] Poor model observability can stem from a variety of system components, including

1) missing physical processes,
2) incommensurate scales of observation and modeling, and
3) inaccurate or arbitrary parameterizations of physical processes.

This study contributes to the community's understanding of soil moisture observability by investigating issues related to items 2 and 3. These components are intrinsically linked because, for example, when heterogeneity cannot be resolved at a given model scale, it must be parameterized.

In situ and remotely sensed soil moisture observations have different horizontal and vertical support volumes than those of LSMs. In situ probes collect data at the centimeter scale, while LSMs typically use kilometer-scale grid cells. Data from high-quality soil moisture networks can be upscaled to match the horizontal scale of a model, but they still typically consist of probes placed at 5-cm depth (Jackson et al. 2012; Colliander et al. 2017a) and thus are sensitive to soil moisture content between approximately 3.5 and 6.5 cm (Rondinelli et al. 2015). LSMs, on the other hand, commonly implement a surface layer that spans 0–10-cm depth (Chen and Dudhia 2001; Niu et al. 2011). While these two volumes are highly correlated, the nonlinear nature of soil moisture may allow for systematic mismatches between the two quantities. Modern remote sensing platforms that utilize L-band radiometers such as NASA's Soil Moisture Active Passive (SMAP) are useful in part because they provide soil moisture at a horizontal scale (10s of kilometers) similar to that of LSM simulations (Kerr et al. 2010; Entekhabi et al. 2014). Vertical support scale, however, still differs (Fig. 1). While nominally reported to be 5 cm (Kerr et al. 2010; Entekhabi et al. 2014), the actual sensing depth is often shallower and depends on soil moisture content, soil texture, surface roughness, and vegetation cover (Liu et al. 2013; Njoku and Kong 1977; Escorihuela et al. 2010; Jackson et al. 2012; Babaeian et al. 2019). The shallower sensing depth is known to affect characterizations of soil drying behavior (Shellito et al. 2016a). To address the inconsistency between modeled and remotely sensed soil depths, some studies have decreased LSM surface layer thickness from 10 to 5 cm or less (Gutmann and Small 2010; Santanello et al. 2019; Santanello and Carlson 2001).

A second source of systematic error comes from the nature of models themselves. The scale of real-world soil moisture heterogeneity is much smaller than that of an individual model grid cell, and LSMs must parameterize processes such as infiltration, evaporation, and runoff to depend on a single soil moisture value for each cell (Koster and Milly 1997). Though such a value may produce reasonable simulations, it may not actually exist in the real world. Therefore, LSM-generated soil moisture quantities can more accurately be considered model-specific indices that must simultaneously characterize each grid cell's aerially averaged soil moisture and the effects of within-grid moisture variability on surface fluxes (Koster et al. 2009; Van Looy et al. 2017). Moreover, model-specific parameterizations ensure that soil moisture from one model cannot be directly used by another without disrupting other states and fluxes (Koster et al. 2009). Similarly problematic is the somewhat arbitrary assignation of soil parameters that are meant to capture real influences of soil texture and have an outsized effect on modeled soil moisture (Ahuja et al. 2010; Lehmann et al. 2018; Gutmann and Small 2007; Xia et al. 2015). We must therefore expect any adjustment that affects soil moisture state to also affect other modeled states and fluxes.

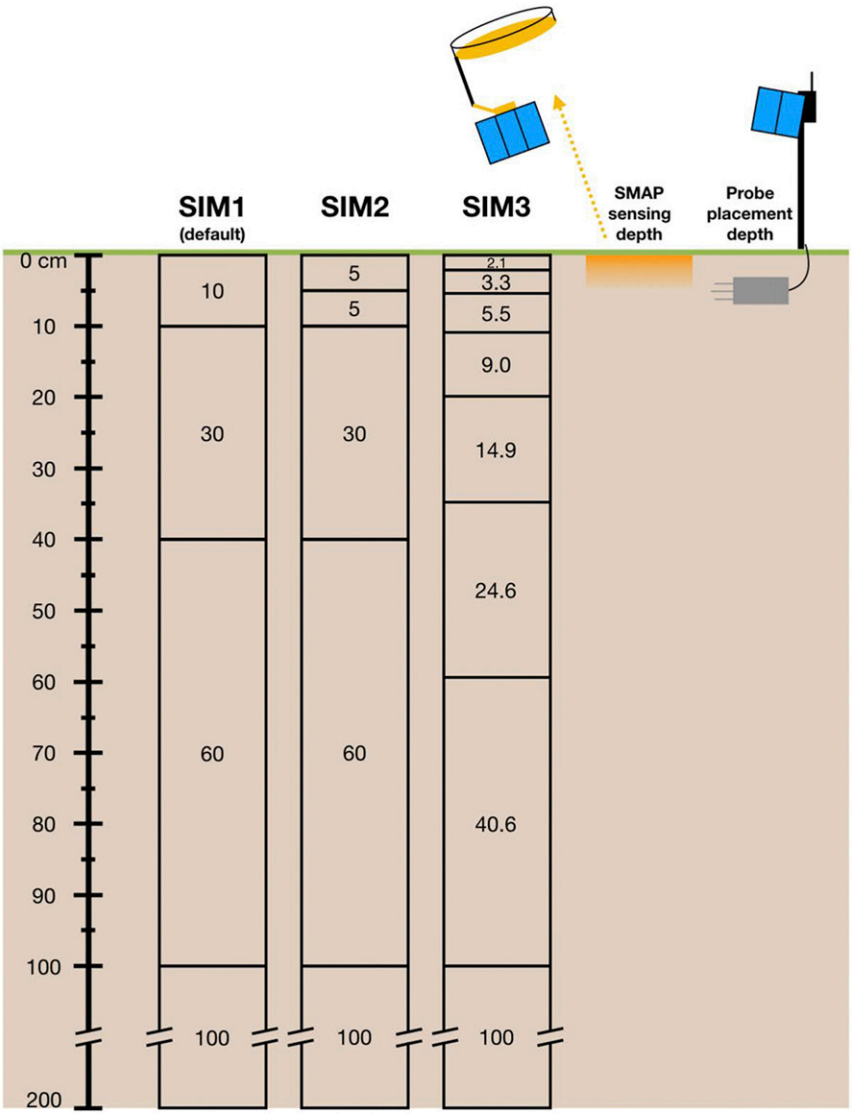

FIG. 1. Schematic showing SMAP L-band sensing depth, 5-cm in situ probe placement depth, and simulation layering schemes for Noah and Noah-MP. All values are in centimeters.

Like LSMs, high-quality soil moisture observations from remote sensing platforms may too include modeled or parameterized components in their retrieval algorithms. Datasets used by observational platforms may be different from data used within an LSM, which provides for another source of bias. For example, SMAP soil moisture products require an inverse τ–ω model, soil and canopy temperature states from NASA Goddard Earth Observing System Model, MODIS-derived land cover class and vegetation water content, and global soil texture characterizations (Entekhabi et al. 2014). SMAP soil moisture is therefore not a direct observation of soil moisture, but rather an estimate based on observed microwave brightness temperature (Tb) and radiometric theory. It contains its own parameterizations and biases.

Fortunately, observations and LSMs can provide scientific insights despite systematic errors and LSM-specific parameters (Kumar et al. 2018). Prior to DA, it is common to rescale observations such that they match the first and second (or higher) statistical moments of the LSM time series. This can be done via normal-deviate-based scaling (Crow et al. 2005) or cumulative distribution function (CDF) matching (Reichle and Koster 2004; Atlas et al. 1990; Anagnostou et al. 1999; Wood 2002). Scaled observations become indicators of anomalous conditions and are useful even if the unscaled observations have a persistent bias.

Alternatively, LSM values can be adjusted toward observations by calibrating model parameters. But a priori calibration of soil moisture on a continental scale is limited by the spatial extent of observations and can introduce errors in associated fluxes (Shellito et al. 2016b). In addition, as discussed above, remotely sensed products can contain modeled information, so calibrating to such observations would not necessarily result in an unbiased LSM time series.

Scaling observations or calibrating LSMs can introduce significant statistical errors if the underlying climatologies are not steady. Unmodeled seasonal irrigation activities may reshape the CDF of the observed soil moisture during part of the year. Without a priori knowledge of watering schedules, the value of observations diminishes (Kumar et al. 2015). It is for this reason that efforts have been made to develop irrigation models that mimic real-world practices (Ozdogan et al. 2010; Lawston et al. 2017a). SMAP is one way to capture irrigation signals, which paves the way for incorporating it into LSMs via DA (Lawston et al. 2017b).

In this study, we delve further into the two causes of poor observability enumerated above: incommensurate scales, and arbitrary parameterizations. To this end, we employ the Noah and Noah-MP LSMs (Chen and Dudhia 2001; Niu et al. 2011) with finer vertical discretization than they contain by default, so that the layering schemes provide surface soil moisture (SSM) quantities that are commensurate with the depth of L-band observations.

In both models, evaporation is designed to pull water from the top soil layer, which results in strong coupling between SSM and evaporation. However, in Noah-MP (but not Noah), the thickness of the surface layer is a parameter in its evaporation formulation (Sakaguchi and Zeng 2009). This means that a change to surface layer thickness will affect Noah-MP SSM content via two mechanisms—a different volume of soil being characterized and a different parameterized rate at which moisture evaporates from that volume. In Noah, SSM is expected to be affected only by the different volume being characterized.

We compare LSM simulations to in situ soil moisture observations from USDA experimental watersheds and to remotely sensed soil moisture retrievals from SMAP. We also quantify how layering schemes affect simulated microwave Tb, a quantity that depends largely on soil moisture and soil temperature. By analyzing Tb values, we are able to compare LSM modeled data to direct SMAP measurements, bypassing the need for the soil moisture retrieval algorithm and the potentially biased ancillary data therein. Through this work, we address the following scientific questions:

1) To what extent and by what mechanism does using a thinner LSM surface layer change soil moisture and Tb simulations?
2) How often does such a change improve the agreement between LSM and observation-based soil moisture and Tb?
3) Where present, do improvements result from a decreased bias, an improved distribution shape, or both?

An improved understanding of the sources of systematic errors between models and observations works toward the broader goal of moving the two into closer agreement and decreasing the community's dependence on rescaling techniques. Such a shift will allow for more effective leveraging of state-of-the-art observational datasets such as SMAP.

2. Models and observations

This study employs NASA's Land Information System (LIS; http://lis.gsfc.nasa.gov/; Kumar et al. 2006; Peters-Lidard et al. 2007) software to conduct the modeling components of the investigation. LIS allows flexible coupling of a suite of land surface models to observationally driven forcing and parameter datasets for benchmarking and data assimilation studies. It comprises three stand-alone components: the Land Surface Data Toolkit (Arsenault et al. 2018a) sets up the static parameters used by the models; LIS (Kumar et al. 2006; Peters-Lidard et al. 2007) coordinates the forcing data and executes the models; and the Land Surface Verification Toolkit (Kumar et al. 2012a), generates statistics from the model output and observational datasets. The LIS modeling framework is publicly available on GitHub (https://github.com/NASA-LIS/LISF).

In section 2a, we describe the LSM setups and forcing data. Section 2b describes the radiative transfer model that has been coupled to the LSMs. Remotely sensed and in situ data are described in sections 2c and 2d, respectively.

a. *Land surface models*

The Noah LSM version 3.3 (Chen and Dudhia 2001; Ek et al. 2003) and its next-generation counterpart, Noah-MP version 3.6 (Niu et al. 2011; Yang et al. 2011), provide estimates of soil moisture, temperature, and turbulent fluxes using four distinct soil layers. We run both models using identical domains, resolutions, land surface parameter datasets, and forcing data. Soil texture designations are taken from the State Soil Geographic Database (STATSGO) from the U.S. Department of Agriculture—Natural Resources Conservation Service (Miller and White 1998). Dominant vegetation types are

TABLE 1. Noah-MP options used in this study. For complete list of available parameterization options, see Arsenault et al. (2018b). For further details regarding each process, see Niu et al. (2011).

Physical process	Parameterization option
Leaf dynamics	Use prescribed LAI and shade fraction
Canopy stomatal resistance	Ball–Berry (Ball et al. 1987)
Soil moisture factor for stomatal resistance	Noah type (Chen et al. 1996)
Runoff and groundwater option	SIMGM (Niu et al. 2007)
Surface layer drag coefficient option	Monin–Obukhov (Brutsaert 1982)
Supercooled liquid water	Standard freezing point depression (Niu and Yang 2006)
Frozen soil permeability	Use total soil moisture to compute hydraulic properties (Niu and Yang 2006)
Radiation transfer option	Modified two-stream with 3D canopy structure (Niu and Yang 2004)
Snow surface albedo	CLASS (Verseghy 1991)
Rainfall and snowfall partitioning	Based on Jordan (1991)

taken from the University of Maryland's land cover classifications (Hansen et al. 2000). The models are forced with meteorological data from NLDAS-2 primary forcing fields, which are available at 1/8° over the CONUS (Xia et al. 2012). Simulations span the 3-yr period of 1 April 2015–1 April 2018, following a 10-yr spinup. Model resolutions are set to match the 1/8° forcing data, and their domains cover the continental United States (CONUS). Noah-MP is capable of a variety of implementation options. We use the setup described in EXP5 of Yang et al. (2011), which takes advantage of all Noah-MP augmentations except the dynamic vegetation scheme (Table 1).

While many aspects of Noah and Noah-MP are similar, their treatment of evaporation is notably different. As shown below, evaporation in Noah depends only on vegetation cover, atmospheric demand for moisture, and SSM supply. In Noah-MP, it is also dependent upon the model's surface layer thickness, a quantity that will be manipulated over the course of this study's experiments. Therefore, to properly understand the impact of our experiments on SSM, we must first inspect the two evaporation mechanisms.

Evaporation in the two models is meant to capture "the real process whereby as bare soil dries, the top few millimeters of the soil become significantly drier than the several centimeters below and thus act as a capping evaporative "crust" barrier at the upper boundary of the topmost soil layer" (Ek et al. 2003). In Noah, this is accomplished with a single empirical parameter, denoted fx, which is set to 2. The evaporation term E_{dir} is formulated as (Ek et al. 2003)

$$E_{\text{dir}} = (1 - \sigma_f) \times \text{FX}^{\text{fx}} \times E_p, \tag{1}$$

where σ_f is fractional vegetation cover (prohibiting evaporation beneath the canopy), FX is relative degree of saturation, and E_p is potential evaporation rate. The squared term results in evaporation rates that drop off quadratically as the top layer's moisture content decreases, approximating the expected effect of a dry crust barrier.

In Noah-MP, evaporation is allowed both over bare soil and beneath the canopy. It depends on the vapor pressure gradient between the air above the ground and the air in the soil where the water vaporizes. Additionally, it depends on aerodynamic resistance and soil resistance (Sakaguchi and Zeng 2009). The soil resistance parameter in Noah-MP r_{soil} more explicitly accommodates for the formation of a dry crust barrier by approximating molecular diffusion through the dry part of the soil:

$$r_{\text{soil}} = \frac{L}{D} \tag{2}$$

where L is the dry layer thickness and D is the vapor diffusivity within the soil (Sakaguchi and Zeng 2009). The dry layer thickness depends directly on the overall thickness of the model's surface layer d_1:

$$L = d_1 \frac{\exp\left[\left(1 - \frac{\theta_1}{\theta_{\text{sat}}}\right)^w\right] - 1}{e - 1}. \tag{3}$$

This means that in contrast to Noah, a change to surface layer thickness in Noah-MP will have a direct impact on evaporation rates. The other parameters in Eq. (3) are θ_1, the soil moisture content of the top model layer; θ_{sat}, the saturated soil moisture content of the soil; w, a concavity parameter that has been empirically determined to be 5; and e, which is the constant 2.718 (Sakaguchi and Zeng 2009).

b. Radiative transfer model

To simulate the raw measurements made by microwave remote sensing instruments, a radiative transfer model (RTM) is coupled with the LSMs used here, similar to the approach in Kumar et al. (2014b). Specifically,

we couple Noah and Noah-MP to the Community Microwave Emission Modeling platform, version 3.0 (CMEM3) (Holmes et al. 2008; Drusch et al. 2009) within the LIS framework. CMEM3 provides estimates of vertically and horizontally polarized microwave Tb using a zero-order τ–ω RTM. It includes contributions from the surface layer of the soil (or snow if present), vegetation, and atmosphere. Because atmospheric effects are removed from SMAP Tb as part of L1 processing (De Lannoy et al. 2015), the LIS implementation of CMEM3 excludes atmospheric emission and absorption. A detailed description of the RTM is provided in the supplemental material.

c. SMAP retrievals and products

SMAP has a sun-synchronous orbit with overpasses at 0600 and 1800 LT. We used morning and evening Tb (both polarizations) and the baseline SSM (SCA-V) from SMAP's level 3 enhanced product [L3SMP_E; Chan et al. (2018), version 2, available through the National Snow and Ice Data Center (NSIDC)]. This product takes advantage of overlapping radiometer footprints to provide retrievals at 33-km resolution posted to a 9-km EASE-Grid 2.0 (Chan et al. 2018). We regridded SMAP products onto the same 1/8° NLDAS-2 grid of the Noah and Noah-MP simulations via nearest neighbor. We removed data that have been flagged due to dense vegetation, mountainous terrain, frozen or snow-covered ground, heavy precipitation, and static water bodies.

The radiometer on board SMAP observes Earth's L-band (1.41 GHz) microwave Tb every 1–3 days (Entekhabi et al. 2010). The algorithm used to extract soil moisture from SMAP Tb requires solving the τ–ω model for soil emissivity (Ulaby et al. 1981; Jackson and Schmugge 1991), then solving the Fresnel equations for soil dielectric (Entekhabi et al. 2014), and finally using a dielectric mixing model (Mironov et al. 2009) to estimate 0–5-cm soil moisture (O'Neill et al. 2018). These submodels require various ancillary data. The τ–ω model utilizes effective surface temperature from Global Modeling and Assimilation Office (GMAO) forecasts (Entekhabi et al. 2014). Its eponymous parameters τ (vegetation optical depth) and ω (single scattering albedo) depend on vegetation water content (VWC), vegetation structure, and microwave frequency and polarization (Entekhabi et al. 2014). Parameter τ is estimated to be linearly proportional to VWC via a land cover look up table, and ω is set to 0.05 globally (O'Neill et al. 2018). VWC itself is estimated from a satellite-based normalized difference vegetation index (Entekhabi et al. 2014). Soil roughness is accounted for using the root mean squared surface height (Choudhury et al. 1979; Wang 1983), which is also estimated from a land cover type lookup table (O'Neill et al. 2018). Due to its better performance at validation sites, the current baseline soil moisture algorithm utilizes vertically polarized microwave radiation (Chan et al. 2016).

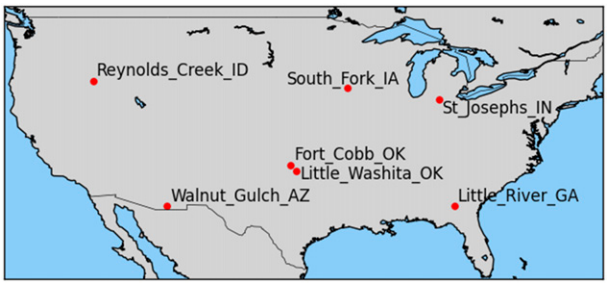

FIG. 2. Locations of the seven densely instrumented SMAP calibration/validation sites used in this study.

To properly address observability, we also compared simulated Tb (from the LSMs plus RTM described above) to SMAP Tb observations. To ensure consistency of Tb values, we use SMAP Tb that has been water-body corrected using ancillary data (part of L1 processing to mitigate against erroneously cool observations caused by the presence of open water within the radiometer footprint) (O'Neill et al. 2018). In addition, both SMAP and the model provide horizontally and vertically polarized Tb values. To capture information from both data streams while maintaining simplicity in our analyses, we averaged the two polarizations together into a single time series. This framework accommodates for the potential of future soil moisture algorithms to incorporate both polarizations (e.g., Chaubell et al. 2020).

d. In situ observations

We focus our study on seven U.S. Department of Agriculture Agricultural Research Service (USDA-ARS) watersheds in the CONUS (Fig. 2). These locations all contain a distributed network of Stevens Water Hydra Probes placed horizontally at 5-cm depth. Individual in situ measurements have been upscaled to 36 km using Voronoi diagrams such that the weighted average soil moisture is commensurate with the scale of SMAP retrievals. These sites are all members of the calibration and validation program for SMAP, meeting a minimum threshold for accuracy and representativeness (Colliander et al. 2017a). Analyses compare upscaled in situ observations against the SMAP and LSM pixels that most closely align with each location. Watersheds span a variety of soil types, land covers, and climatic regimes. Further details and descriptions of each site can be found in

Colliander et al. (2017a), and datasets are available from Colliander et al. (2017b).

3. Methods

a. Model configurations

We conducted three numerical experiments with both Noah and Noah-MP. Each has a different number of soil layers as illustrated in Fig. 1. SIM1 uses the default Noah LSM configuration. SIM2 includes one additional layer, obtained by evenly splitting the top layer. The 5-cm surface layer of SIM2 thus provides an exact match with the nominal sensing depth of an L-band radiometer (Kerr et al. 2010; Entekhabi et al. 2014). SIM3 uses a finer discretization based on the exponential spacing described in the Community Land Model (Brunke et al. 2016). Our implementation places seven layers in the first 100 cm and keeps the bottom layer thickness at 100 cm. The SIM3 setup provides a surface layer thickness of 2.1 cm, which may be a more accurate characterization of L-band radiometer sensing depth (Escorihuela et al. 2010; Liu et al. 2013).

As shown in section 2a, adjustments to surface layer thickness directly affect evaporation rates in Noah-MP. While we do not intend to introduce a new version of that model, we briefly present Noah-MP simulations wherein d_1 in Eq. (3) was hard-coded to 10 cm. The three experiments shown in Fig. 1 were repeated, providing a set of simulations wherein evaporation and surface layer thickness were linked only through the layering schemes' impact on SSM. Note that because SIM1 has a surface layer thickness of 10 cm already, hard coding d_1 in this way did not affect that simulation.

In Noah and Noah-MP, vegetation rooting depths are defined as the number of model layers (starting from the top) in which roots exist. To obtain consistent rooting depths across all experiments, we increased the number of layers in which roots are found for SIM2 and SIM3. Our modifications maintained the full 200-cm rooting depth for tree-covered land and 100-cm rooting depths for croplands, shrublands, and grasslands. A slight compromise had to be made when defining rooting depths in the "bare soil" and "urban" classes: SIM1 and SIM2 define these roots (when present) to reach 10 cm, but the closest layer interface available in SIM3 is at 10.9 cm. Because of the inherent lack of vegetation in these classes, we do not expect this slight modification to significantly affect our results.

b. Quantifying agreement

This study used soil moisture and Tb values to show and quantify the agreement between models and observations. We directly compared pairs of empirical CDFs (eCDFs) from the LSMs, SMAP, and in situ probes. To ensure that each dataset covered the same temporal and spatial domain, time periods and locations that did not include a valid SMAP retrieval were omitted.

We quantified eCDF agreement using the two-sample Kolmogorov–Smirnov (KS) test (Chakravarti et al. 1967). The KS statistic is defined as the largest distance between two eCDFs and ranges from zero (exact match) to one (distributions have no overlap). Previous hydrologic studies have used the KS test in a similar way to provide insight into first, second, and higher-order statistical moments through a single value (Kumar et al. 2015; Jaeger and Seneviratne 2011; Zhang et al. 2018). A second metric we employed in this study was the overall mean difference between observed and modeled time series. Through this measure, we gained first-order insight into the effect each experiment had on the magnitude of simulated values. Last, we determined unbiased KS values by implementing the KS test on pairs of eCDF that had had their mean values removed. This metric provided information about how closely the *shapes* of two eCDFs curves agreed with one another, independent of any bias that may have existed. Unbiased KS values are affected by standard deviations and higher-order statistical moments.

In most analyses, the data we used to generate eCDFs are SMAP soil moisture, in situ soil moisture, and SSM from the models. As shown in Fig. 1, the depth intervals characterized by each data source are not identical. L-band radiometers are sensitive to soil moisture between the surface and a (variable) depth of 2–5 cm, so when comparing SMAP retrievals to models, we utilized only the top layer of each model. In these analyses, the match between SMAP and the relatively thick layer 1 in SIM1 is more approximate than that between SMAP and the thinner layer 1 of SIM2 or SIM3. The sensing depth of in situ moisture probes is also inexactly characterized by the LSM configurations. The logical match for 5-cm probe placements is a 0–10-cm model interval, which is symmetrical around the few centimeters of soil to which the probe is sensitive. Therefore, for consistency, we also compared in situ probes to 0–10-cm soil moisture quantities in SIM2 and SIM3. For SIM2, this required averaging layers 1 and 2. For SIM3, we used a weighted average of layers 1–3, which provided 0–10.9-cm soil moisture. In this way, we explicitly quantify the role of model vertical resolution.

As described in section 2c, a true assessment of LSM observability must be conducted in Tb observation space in addition to soil moisture space (where ancillary data are tied to the SMAP product). Our analyses utilize Tb from SMAP and from the coupled LSM+RTM

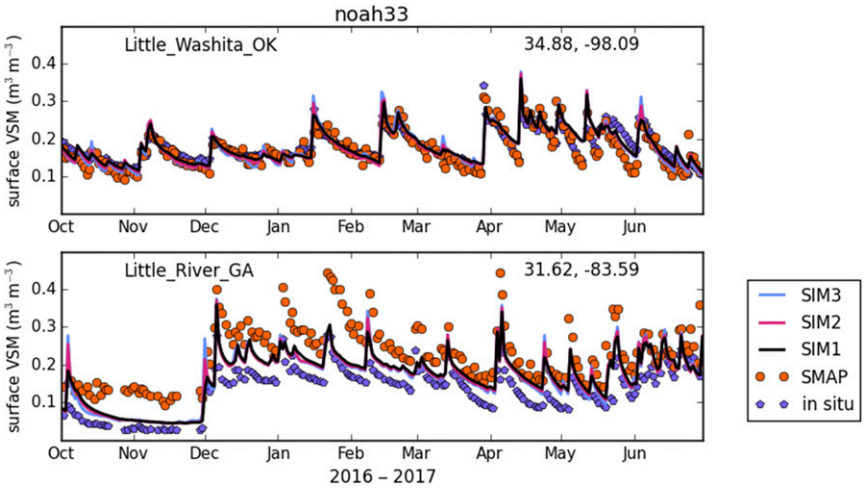

FIG. 3. Surface layer soil moisture at Little Washita, OK, and Little River, GA. Noah SIM1, SIM2, and SIM3 are shown in black, pink, and blue, respectively. SMAP soil moisture retrievals are marked with orange circles. Basin-averaged 5-cm in situ probe data are marked with purple pentagons.

models (section 2b). These Tb analyses remove the burden of RTM parameterizations from SMAP and place it instead on the models.

Most of our analyses focused on the seven USDA-ARS watersheds described in section 2d. These sites have high-quality in situ soil moisture data against which we can assess LSM SSM. We also analyzed SMAP and LSM data from SIM1 and SIM3 at 1/8° over the CONUS to gain insight into how these two layering configurations affect distributed SSM and Tb. In all cases, we calculated KS values, mean differences, and unbiased KS values between simulations and observations.

4. Results

Surface layer thicknesses vary across SIM1, SIM2, and SIM3. Accordingly, different depths contribute to the moisture and Tb values shown in these results, with the exception of section 4d, where we analyze soil moisture from the same 0–10-cm depth across all three experiments.

a. Noah SSM time series

Figure 3 shows a portion of the SSM time series from Noah, Noah-MP, SMAP, and in situ observations at two of the USDA-ARS watersheds. These two locations demonstrate the spread and inconsistency of soil moisture from each source. Little Washita, Oklahoma (OK), shows excellent agreement between simulations, in situ observations, and SMAP retrievals, while Little River, Georgia (GA), shows moisture levels to be consistently different between each source. Differences in mean values are also found to varying degrees in the other five watersheds (Fig. S1, Table S1 in the online supplemental material), highlighting the need for bias correction approaches if observational data were to be assimilated into this LSM.

Shortening the surface layer in Noah has a negligible effect on SSM at most times and locations. Thinner surface layers allow for slightly more thorough wetting by precipitation events, as the same volume of rain is distributed throughout a thinner soil volume. This effect can be seen at most soil moisture peaks, such as at Little Washita, OK, in early June 2017. The excess moisture, however, is short lived. It drains, diffuses, or evaporates out of the surface layer quickly enough that within a day, the moisture levels of SIM2 and SIM3 are again indistinguishable from those of SIM1.

b. Noah-MP SSM time series

Figure 4 shows SSM simulated by Noah-MP at the same two watersheds. The baseline simulation (SIM1) is similar to that of Noah (Fig. 3), with minor discrepancies due to inherent differences in the physics of the two models. These two sites (and all sites except Walnut Gulch; Fig. S2) show SSM from Noah-MP SIM1 to be wetter than SSM from Noah SIM1.

The three Noah-MP experiments exhibit noticeably larger differences between them than Noah simulations do. By overlaying soil evaporation volumes onto Fig. 4 (dotted lines), we show that SIM3 contains evaporation biases up to ~25% above SIM1. (Transpiration volumes remain virtually identical across the three experiments and are smaller in magnitude than evaporation—not

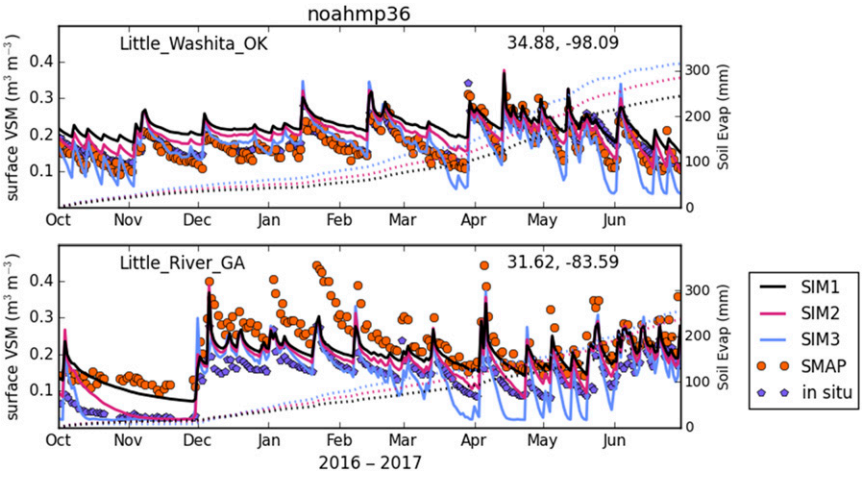

FIG. 4. As in Fig. 3, but for Noah-MP simulations. Accumulated soil evaporation for each simulation is shown with the same color using dotted lines and the right axis.

shown.) Because evaporation (described in section 2a) pulls moisture only from the surface soil layer, we expect inflated evaporation volumes to result in commensurate decreases in simulated SSM values. We test the extent of this linkage by repeating the three experiments after hard-coding d_1 in the Noah-MP evaporation scheme to 10 cm (further described in section 3a).

Figure 5 shows Noah-MP results at the same two watersheds after implementing the one-line change to Noah-MP. (Other site time series are shown in Fig. S3.) In contrast to Fig. 4, the modified Noah-MP results of Fig. 5 exhibit similar soil evaporation volumes and SSM across the three experiments. Remaining differences in SSM only exist at the moisture peaks (such as early June at Little Washita, OK) and during extended dry downs (such as November at Little River, GA). Together, Figs. 4 and 5 confirm that the direct dependence of Noah-MP's bare soil evaporation scheme on surface layer thickness is the dominant mechanism behind the differing Noah-MP SSM time series shown in Fig. 4. However, for consistency, the remainder of this study is conducted using the unmodified Noah-MP surface evaporation scheme.

c. *SSM cumulative distribution functions*

The time series of SSM provided in sections 4a and 4b can be more quantitatively described using eCDFs, from which we derive KS distance values and mean differences. In Fig. 6, we show eCDFs of simulations and observations using all three years of data. As before, the

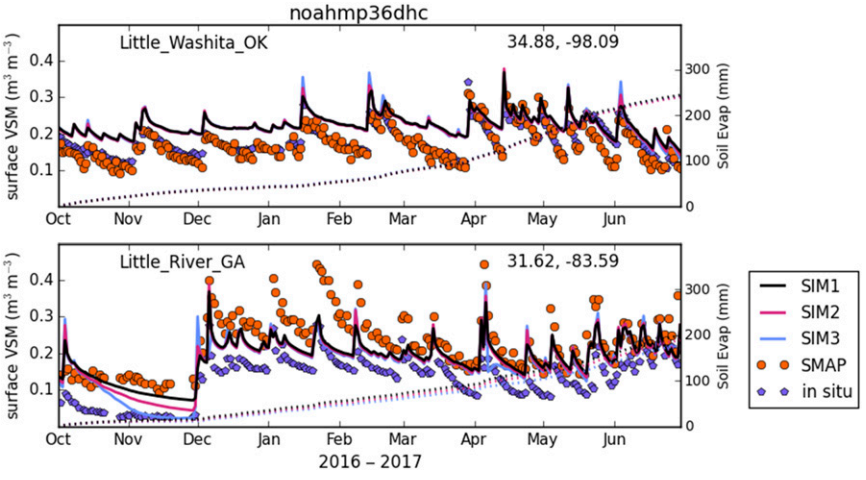

FIG. 5. As in Fig. 4, but for Noah-MP with surface resistance hard-coded to use a 10-cm surface layer.

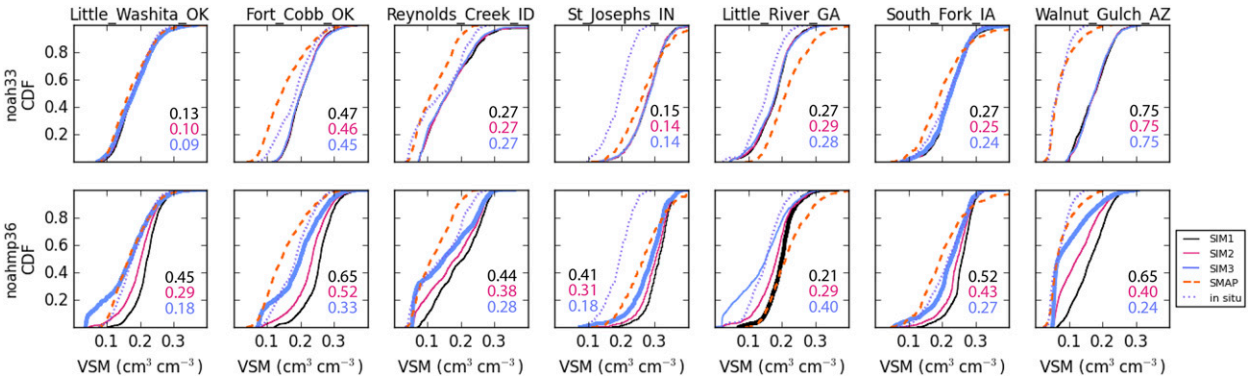

FIG. 6. eCDFs of SSM from Noah and Noah-MP simulations, SMAP, and in situ probes. KS test values between simulations and SMAP retrievals are shown according to simulation color. Thick lines indicate instances where the KS value of one simulation is at least 1% better than the other two. Mean differences and other KS test values are provided in Table S1.

Noah simulations show little sensitivity to changes in surface layer thickness. Noah-MP exhibits noticeably drier SSM when the thinner configurations are used, especially on the dry end of the distribution. Table S1 contains KS values and relative mean differences derived from these eCDFs and indicates which of the three layering configurations provides the best match between modeled SSM and SMAP or in situ observations.

In Noah simulations, the KS values of the three experiments' SSM compared to SMAP SSM and in situ soil moisture are quite similar, confirming the qualitative assessment made in section 4a. When nontrivial differences do exist, SIM3 eCDFs demonstrate a slightly better match against observations than those from SIM1 and SIM2. The only exception is at Walnut Gulch, Arizona (AZ), where SIM2 and SIM3 are both slightly worse than SIM1 when compared to in situ soil moisture. Mean differences between LSMs and both SMAP SSM and in situ soil moisture are positive (LSM is wetter) at all sites except Little River, GA, where the LSM is drier than the SMAP retrievals. The mean values are trivially affected by changing layer thicknesses.

In Noah-MP simulations, the KS values (Table S1) show a larger diversity of values, reflecting the different dry down and eCDF shapes shown in Figs. 4 and 6. In all cases but one (Little River, GA), SIM3 (thinnest surface layer; Fig. 1) provides the lowest KS values with respect to both SMAP and in situ soil moisture. Notably, each site that shows SIM3 KS values to improve over those from SIM1 also exhibits a wetter mean SIM1 SSM value than the remotely sensed or in situ observations do. The thinner soil layers of SIM2 and SIM3 reliably decrease that difference and improve the associated KS values. These results allow us to attribute a significant part of the KS test results to differences in mean values between simulations and observations. While the dependence of KS values on mean values is not surprising, it motivates the need to investigate unbiased eCDFs and associated unbiased KS values, which we do in section 4g.

It is also clear from Fig. 6 and Table S1 that there are often nontrivial differences between in situ soil moisture and SMAP SSM. The largest discrepancy is found at St. Josephs, Indiana (IN), where the KS distance is 0.54. [Due to insufficient spatial scale and associated upscaling studies, this watershed is the only one of the seven that has not met the stringent requirements to be designated a "core" cal/val site at the 36-km scale (Colliander et al. 2017a).] Poor agreement of SMAP retrievals with in situ soil moisture guarantees that LSM simulations will be unable to simultaneously match both datasets.

As described in the introduction, the mismatch between SMAP and individual in situ data is in part expected. Problems stem (at least) from the facts that SMAP retrievals include global model parameterizations and characterize a shallower soil depth than the in situ probes do. In the following section, we address the component of in situ–model mismatch that may come from the incongruity of soil depths between probes and models. In section 4f, we address the component of SMAP–model mismatch that may come from the inclusion of modeled data in SMAP retrievals.

d. 0–10-cm cumulative distribution functions

In Fig. 7, we show eCDFs of simulated 0–10-cm soil moisture against the 5-cm in situ observations. The KS values and mean differences derived from these eCDFs are provided in Table S1. Noah simulations again show only slight differences among the three experiments and show no changes to overall means. At St. Josephs, IN; South Fork, Iowa (IA); and Walnut Gulch, AZ, SIM1 0–10-cm soil moisture provides a marginally better

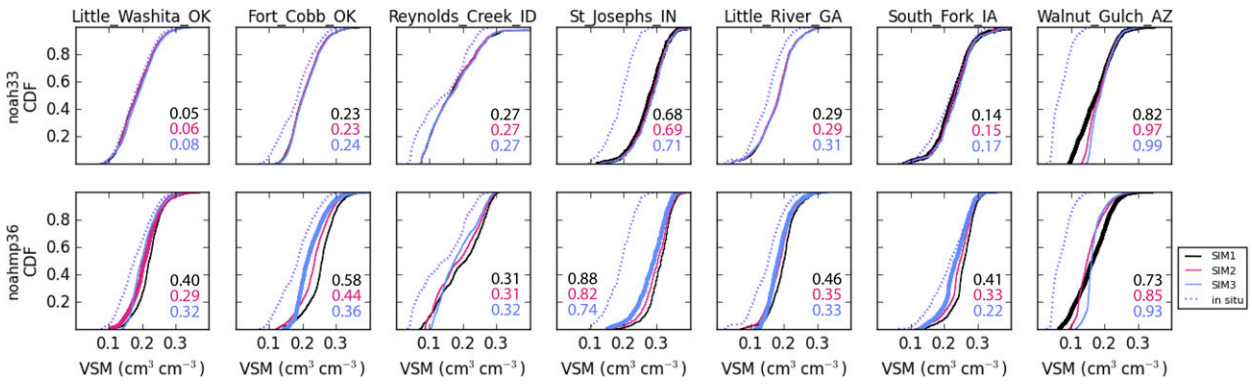

FIG. 7. eCDFs of 0–10-cm soil moisture from simulations and in situ probes. KS test values between simulations and in situ observations are shown according to simulation color. Thick lines indicate instances where the KS test value of one simulation is at least 1% better than the other two. Mean differences are provided in Table S1.

match with in situ observations than the other two simulations do. Agreement among Noah-MP simulations of 0–10–cm soil moisture varies more widely, but not as widely as when only the top layer was considered (section 4c). A majority of the sites are best served using 0–10-cm soil moisture from SIM3, and as before, SIM3 almost always provides soil moisture with the smallest mean difference from the in situ observations. Only at Walnut Gulch, AZ, does the 0–10-cm soil moisture from SIM1 provide a lower KS value than does 0–10-cm soil moisture from SIM2 or SIM3. It is also the only site where the 0–10-cm soil moisture from SIM3 does not provide the smallest mean difference. These results are likely due to the dry climate that facilitates decoupling between the surface soil moisture and layers below it.

Overall, the results from this section show that implementing finer layer discretization's in Noah makes a negligible difference in the eCDF of its 0–10-cm soil moisture. In Noah-MP, the fit between simulated 0–10-cm soil moisture and in situ probes does change between SIM1, SIM2, and SIM3, but to a lesser degree than when only SSM was considered (in the previous section). The fact that at most locations, all three simulations from both models still provide far from perfect agreement with in situ soil moisture indicates that the issue of soil moisture support volume is only a small factor affecting agreement with observations. Instead, changes to mean soil moisture values are again driving the improvements. Evidence to this effect comes from Noah-MP simulations, where at all sites there is a better match (lower KS value) between in situ soil moisture and the surface layers of SIM2 and SIM3 than between in situ soil moisture and the 0–10-cm average from SIM2 and SIM3. (Those two quantities are identical in SIM1.) That result is puzzling considering that neither the 0–2-cm interval nor the 0–5-cm interval spans the actual placement depth of the in situ probes (5 cm). But it is explained by the fact that the default model at all sites is wetter on average than the in situ observations (Table S1). Those differences are mitigated by omitting the relatively wetter soil layer 2 (in the case of SIM2) or soil layers 2 and 3 (in the case of SIM3). Better agreement between mean values results in lower KS values and overshadows the effect of the physical incongruity between model simulation depth and in situ probe placement depth.

The dominant role of mean values and relatively small role of support volume suggests that model parameters and parameterizations are more important for observability than the physical agreement between modeled and observed depths. In the next section, we assess the veracity of such a statement by comparing SMAP Tb retrievals and simulated Tb values.

e. Noah and Noah-MP Tb time series

We compare simulated Tb values to SMAP Tb at the same seven locations used in the soil moisture analysis. The overall wetting and drying patterns observed in Fig. 8 (using Noah) and Fig. 9 (using Noah-MP) are inversions of the SSM time series shown earlier. Wet soil corresponds to low Tb because there is a negative relationship between soil moisture and emissivity (Jackson and Schmugge 1989; Jackson et al. 1982). As in Figs. 3 and 4, the differences between SIM1, SIM2, and SIM3 are more distinct in the Noah-MP simulations than in the Noah simulations.

Although the wetting and drying trends shown in Tb space are straightforward, the mean differences between Tb values are notably different from those in soil moisture space. Whereas mean LSM soil moisture values from Little Washita, OK, are negligibly different from SMAP SSM retrievals, the coupled LSM-RTM simulations result in distinctly warmer mean modeled Tb values than SMAP Tb values. Mean Tb differences at

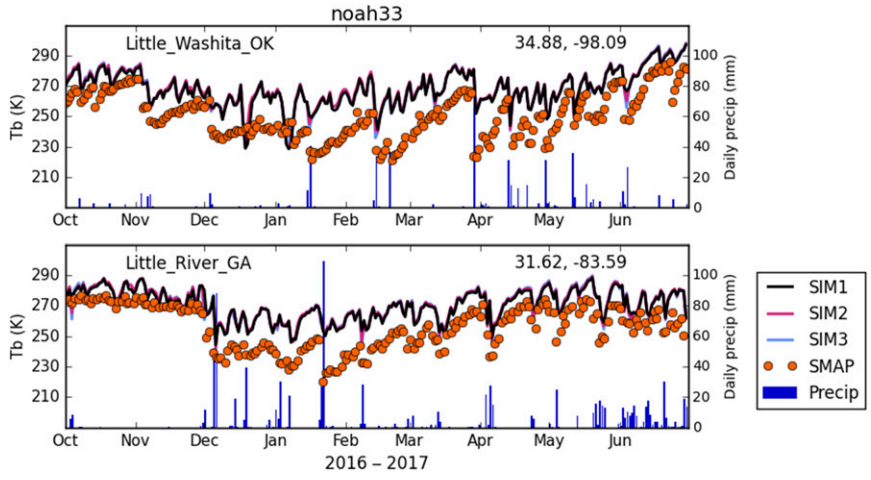

FIG. 8. Tb at Little Washita, OK, and Little River, GA. Noah SIM1, SIM2, and SIM3 coupled to CMEM3 are shown in black, pink, and blue, respectively. SMAP Tb retrievals are marked with orange circles. Daily precipitation is shown with blue bars.

other sites (notably Walnut Gulch, AZ; Fig. S4) also differ in magnitude from mean SSM differences. Part of the difference could be an artifact of the SMAP retrieval algorithm, which utilizes only the vertically polarized microwave signal. H-polarized signals are often cooler, which could lead to a wet-biased soil moisture reading. We investigate these inconsistencies further in the next two sections.

f. Tb cumulative distribution functions

As before, we can quantitatively assess model performance using eCDFs that show simulated and observed Tb from all three years of our analysis (Fig. 10). Noah shows negligible sensitivity of Tb to layering schemes. Noah-MP shows Tb to depend on layering scheme, but with differences that are somewhat muted compared to those observed in soil moisture space (Fig. 6). This tempering is expected, since surface soil moisture is only part of what CMEM3 uses to calculate Tb. Vegetation water content, soil roughness, and soil texture will remain the same between each experiment, forcing some degree of similarity between the three experiments. Overall, Fig. 10 and Table S1 show that Noah-MP simulations with a thinner surface layer (SIM3) result in warmer Tbs than do simulations with the default surface layer thickness (SIM1). This result is internally consistent with SIM3 producing drier soil than SIM1 does (Figs. 4 and 6).

At all sites, when nontrivial differences exist between simulated and observed Tb eCDFs, the best agreement with SMAP Tb is provided by SIM1, the default simulation. (See the bolded black lines of Fig. 10 and

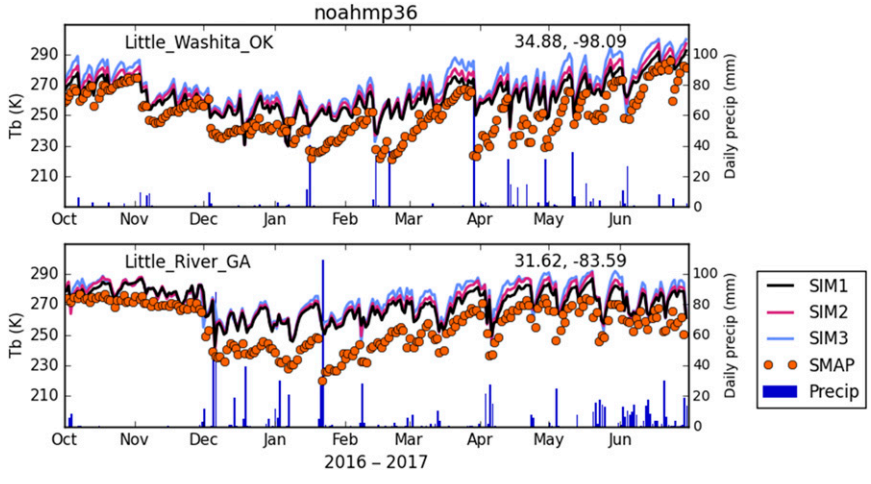

FIG. 9. As in Fig. 8, but using Noah-MP simulations coupled to CMEM3.

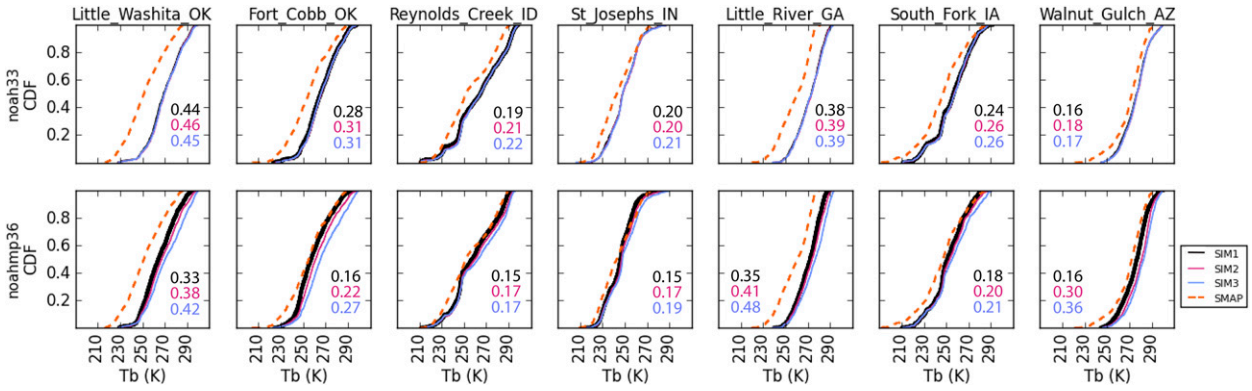

FIG. 10. eCDFs of microwave Tb from coupled LSM-RTM simulations and SMAP. KS test values are shown according to simulation color. Thick lines indicate instances where the KS value of one simulation is at least 1% better than the other two. Mean differences are shown in Table S1.

associated KS values.) This result is in direct contrast to the results shown in section 4c, where SIM3 performs best, and indicates an inconsistency between SMAP's retrieval algorithm and the CMEM3 RTM. Because both use the τ–ω model, the contrasting results must be a consequence of different parameters or submodels. For one, soil reflectivity is determined to depend on soil roughness differently by CMEM3 and SMAP. The former uses the model of Wegmüller and Mätzler (1999) (see supplemental material), whereas the latter utilizes that of Choudhury et al. (1979) (Entekhabi et al. 2014).

The Tb results allow us to qualify the soil moisture results presented in section 4c: SSM from SIM3 was largely shown to provide better agreement with SMAP soil moisture than SIM1, but at least part of that result is due to the initial mean difference between the default simulation and observations. Initial mean Tb differences often do not follow the expected sign inversion from SSM, changing the overall result of implementing thinner surface layers. In soil moisture space, all sites except Little River, GA, show SIM1 as being wetter than SMAP does. But in Tb space, they all show SIM1 as being warmer than SMAP does. By introducing thinner surface layers in SIM2 and SIM3, the SSM difference is reduced, but the Tb difference is exacerbated.

In the following section, we consider the shapes of the eCDF curves themselves and establish the degree to which a thinner model surface layer affects wetting and drying independent of the mean moisture level.

g. *Unbiased cumulative distribution functions*

Figure 11 contains eCDFs of SMAP, in situ, and simulated soil moisture after the long-term mean value from each time series was removed. The unbiased KS values associated with Fig. 11 are contained in Table S1 and characterize how well the shapes of the eCDFs agree with one another. In this way, we remove considerations of how model layering schemes affect mean values and instead assess their impact on soil moisture dynamics alone.

The Noah results show only small differences in dynamics between the three experiments. In most cases, there is less than a 1% change in unbiased KS value between SIM1, SIM2, and SIM3, no matter if it is

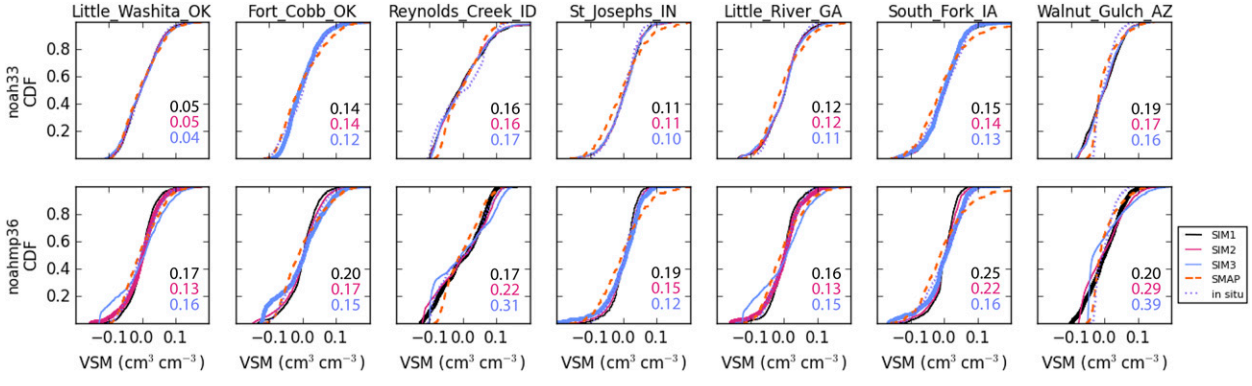

FIG. 11. As in Fig. 6, but with unbiased volumetric soil moisture values.

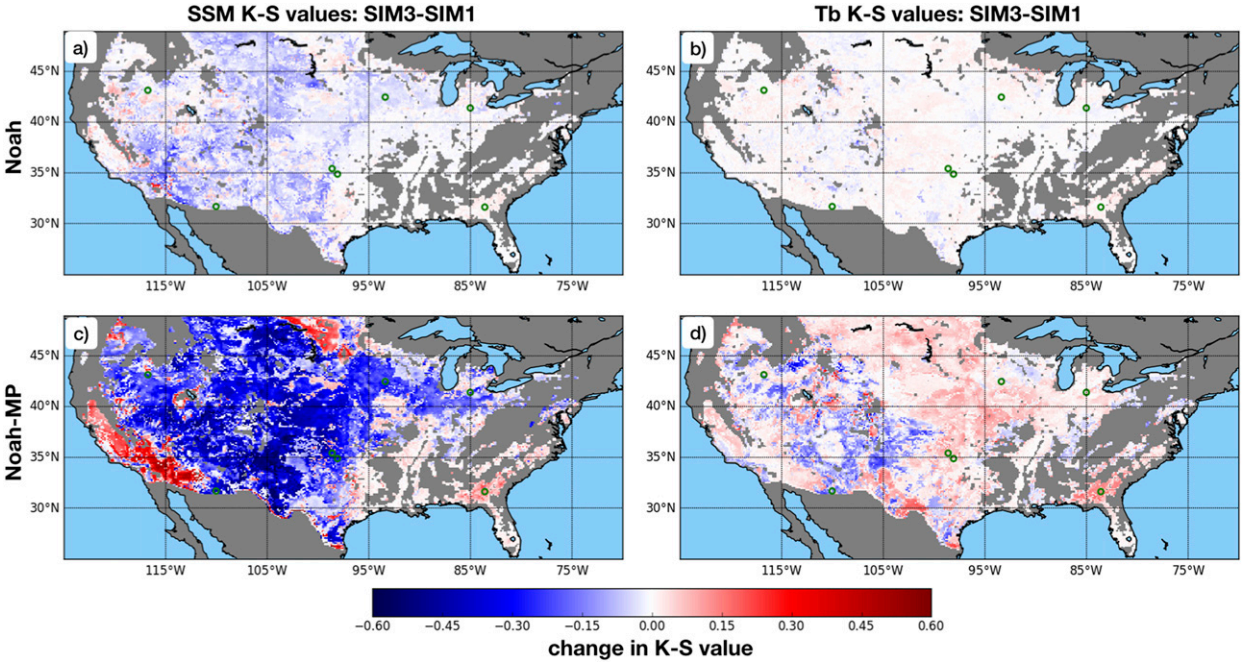

FIG. 12. Improvement (blue) or degradation (red) of observability when SIM3 is used in place of SIM1, as measured by the change in KS value (a),(c) between LSM and SMAP SSM and (b),(d) between LSM-RTM and SMAP Tb. Noah results are shown in (a) and (b) and Noah-MP results are shown in (c) and (d). Locations of the seven study sites are indicated with green circles.

calculated against SMAP SSM or against in situ soil moisture observations.

Noah-MP simulations are more distinct from one another. The unbiased soil moisture eCDFs tend to be flatter with the SIM3 configuration than with the SIM1 configuration. This is apparent at the two Oklahoma sites, among others. The flattening of the curves indicates that the system spends a greater proportion of time with soil moisture values that are further from the mean. This can be accomplished by a widening of soil moisture dynamic range or by a greater sensitivity to wet and dry periods, both of which are consistent with a thinner surface layer that can more thoroughly wet up with rainfall and dry down afterward.

When compared against observations, the performance of Noah-MP simulations is inconsistent. The best agreement with SMAP soil moisture (bolded lines in Fig. 11) is provided by SIM1 at two sites, SIM2 at two sites, and SIM3 at three sites. The best agreement with in situ soil moisture (Table S1) is provided by SIM1, SIM2, and SIM3 at two, four, and one site, respectively.

Though none of the layering schemes is unequivocally better than the other two, the unbiased KS values themselves reveal an important finding. All of the unbiased time series from Noah simulations match SMAP soil moisture better than do all of the unbiased time series from Noah-MP simulations. When compared against in situ data, the same general trend holds, though there are a few exceptions. In other words, Noah provides more realistic moisture dynamics than Noah-MP does, regardless of which of the three layering structures is used. These models share much of their lineage and are forced by the same data. They differ in how various processes are parameterized. Therefore, these results again indicate that the role of model layering schemes on the observability of moisture dynamics is secondary to that of model parameterizations.

h. Distributed SSM intercomparison

In this section, we implemented SIM1 and SIM3 in Noah and Noah-MP over the CONUS and calculated the KS values, mean differences, and unbiased KS values with respect to SMAP soil moisture retrievals and SMAP Tb at each NLDAS pixel. Figure 12 shows the overall improvement or degradation to KS values that results from using the thinner layering configuration of SIM3 instead of the default layering configuration of SIM1. For both SSM and Tb, the Noah-MP results show more intense blues and reds, indicating as before that changes to layering schemes affect Noah-MP simulations much more than they do those from Noah. The preponderance of blue in Figs. 12a and 12c indicates that using a thinner surface layer improves agreement between modeled SSM and SMAP SSM in more locations than it degrades it. However, the fact that Fig. 12b and especially Fig. 12d contain more red than blue indicates

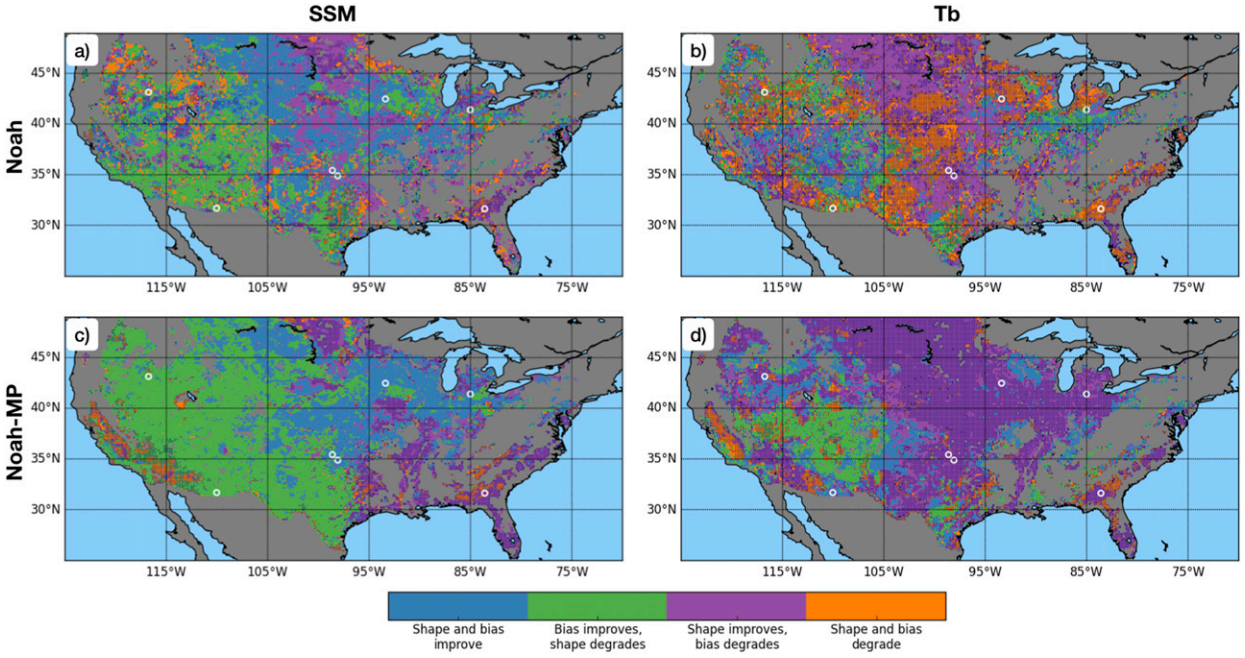

FIG. 13. Components of observability [mean difference (bias) and unbiased KS value (shape)] that were improved or degraded when SIM3 was used in place of SIM1. Metrics are calculated (a),(c) against SMAP SSM and (b),(d) against SMAP Tb. Noah results are shown in (a) and (b) and Noah-MP results are shown in (c) and (d). Stippling indicates pixels where the KS value of SIM3 was worse than that of SIM1. Locations of the seven study sites are indicated with white circles.

that agreement of Tb between SIM3 and SMAP is worse than that between SIM1 and SMAP. These conflicting results were also found in the site-specific analyses (section 4f).

In Fig. 13, we categorized each pixel according to whether its mean value and/or its unbiased KS value compared to SSM and Tb observations were improved or degraded when switching from SIM1 to SIM3. In this way, we quantified on a continental scale the relative effect of each component on SIM3 performance.

Both models exhibit a reduction in mean SSM difference from SMAP over a majority of the country when SIM3 is used instead of SIM1 (blue and green pixels in Figs. 13a and 13c). Such pixels cover wide swaths of the West and Midwest, especially for Noah-MP. The same cannot be said about mean Tb differences: blue and green areas in Figs. 13b and 13d constitute a minority of the CONUS pixels and are predominantly limited to arid regions of the country. Such regionally dependent results may reflect differences in L-band sensing depth, which is shallower when more vegetation is present, and deeper over bare soil (Babaeian et al. 2019).

Improvements to unbiased SSM KS values, which indicates agreement of eCDF shape between models and observations, are found in humid and semiarid regions of the CONUS (blue and purple pixels). Improvements to unbiased Tb KS values are found throughout the CONUS especially as simulated by Noah-MP. In one respect, this result is encouraging because it indicates that Tb dynamics of SMAP are more accurately produced with a model that contains a 2-cm surface layer. However, when we consider overall KS value, the improvements to unbiased KS values are vastly overshadowed by the influence on mean model values.

In simulations of both SSM and Tb, pixels where overall KS values worsen (as shown in red in Fig. 12 and with stippling in Fig. 13) largely coincide with increased mean differences (blue and purple pixels). Stated another way, when SIM3 improves upon SIM1, the changes in KS values are largely driven by improvements in agreement between mean values, not by improvements to the eCDF shapes. This is most obvious in Fig. 13d, where in most of the Midwest, using SIM3 in place of SIM1 degrades the agreement between means and improves the unbiased KS value. The stippling indicates that overall KS value has worsened.

5. Discussion and conclusions

This study investigated the potential to improve LSM surface soil moisture observability by increasing layer discretization in Noah and Noah-MP. We carried out simulations at seven densely instrumented watersheds with model surface layer thicknesses set to 10 cm

(default, SIM1), 5 cm (SIM2), and 2 cm (SIM3). We assessed each experiment's effect on soil moisture by calculating KS values, mean differences, and unbiased KS values between LSM simulations and in situ probes and between LSM simulations and SMAP retrievals. In addition, we assessed modeled Tb by coupling the LSMs to an RTM and comparing its output to SMAP Tb observations.

Shortening the models' surface layer thickness allows for more rapid wetting-up of the soil during rainfall and more rapid and thorough drying-out of the soil during dry down periods. In Noah-MP, there is also a decrease in mean SSM levels. These findings are consistent with the intuition behind thinner soil layers acting as a smaller reservoir for the system's inputs of precipitation and outputs of evapotranspiration and drainage. They are also consistent with prior studies that show soil drying to occur more rapidly in near-surface layers than in those that are deeper, such as the 0–10-cm interval typically characterized in LSMs (Santanello and Carlson 2001; Rondinelli et al. 2015; Kurc and Small 2004).

Changing the model soil layering makes a more significant difference in Noah-MP simulations than in Noah simulations. This can be attributed to the fact that the experiments affect Noah soil moisture only via changes to its support volume. SSM in Noah-MP is additionally affected by the parameterization of surface evaporation, which is enhanced as the surface layer is thinned.

In the Noah-MP experiments, a majority of the seven locations analyzed in this study exhibit better KS values between SIM3 SSM and SMAP SSM than between SIM1 and SMAP. SIM2 results in KS values that are intermediate between the two others. Similar results were found when comparing simulated SSM against in situ soil moisture probes, despite their placement at 5 cm, which is deeper than SMAP's sensing depth and deeper than the surface layers of SIM2 and SIM3. The physical incongruity of the in situ results reveals the importance of model parameterizations on the mean values of resultant SSM: KS values can improve merely from decreases in mean moisture levels, in addition to (or even in spite of) changes to higher-order dynamics.

The same experiments implemented in Noah also slightly favor SIM3 over SIM1, both when compared against SMAP retrievals and against in situ soil moisture probes. However, the changes in KS values are often negligible, which shows that more physically realistic layering schemes alone do not drive significant improvements to modeled SSM. Instead, it is the parameterized dependence of surface evaporation on model surface layer thickness in Noah-MP that drives changes to its mean SSM levels and KS values.

The above results are based on analyses of soil moisture. That is, comparisons were made between LSM simulated soil moisture and either in situ soil moisture observations or SMAP SSM retrievals. However, because SMAP soil moisture products require algorithms that use ancillary model data, they are not stand-alone (direct) observations themselves and cannot rightly be used to quantify the observability of LSM soil moisture. To perform a more direct comparison against SMAP measurements, we repeated our analyses in Tb space: coupling the two LSMs to the CMEM3 RTM allowed changes to simulated SSM to propagate to Tb values. As expected, Tb time series are inverted and slightly muted when compared to SSM.

Tb results are quite opposite those found in soil moisture space. Differences in KS values, where present, favor the 10-cm surface thickness of SIM1 instead of the 2- or 5-cm thickness of SIM2 or SIM3. The conflicting results again indicate the importance of model parameterizations and bias structure in quantifying observability. The SMAP retrieval algorithm and the CMEM3 RTM are not exact inverses of one another. They utilize different parameters, submodels, and soil temperatures to convert Tb to SSM and vice versa. The differences are significant enough to affect the sign of the default model's mean value compared to SMAP observations and change whether or not the finer layer discretization of SIM3 provides an improvement over SIM1. Adjustments to model vertical resolution must therefore be implemented with caution: their effect on model bias signatures may not be immediately apparent, but they control the first-order results.

By removing biases a priori and calculating unbiased KS values, we explicitly addressed the effect of changing model layer thicknesses on second- and higher-order statistical moments of soil moisture. In Noah, these effects are negligible at the seven study sites. In Noah-MP, the experiment containing the best unbiased agreement with in situ or SMAP soil moisture is inconsistent and varies by site.

The dominant role that bias has on KS values is further confirmed in the distributed results. Regions of the country whose KS values improve when switching from SIM1 to SIM3 neatly correspond with regions where the mean difference between the LSM and SMAP values also improves, especially in Noah-MP. There are only a limited number of pixels wherein KS values degrade but mean difference improves and vice versa. This CONUS-wide analysis confirms that KS value improvements are almost exclusively driven by shifts in the mean, not by changes to the eCDF shape.

By showing that model biases and observability are driven more by parameters and parameterizations than

by vertical support volume, we emphasize that the role of thinner model layering schemes must be considered within the larger context of limitations in soil physics and parameters. The fact that 0–2-cm layers correspond with 5-cm in situ probes better than 0–10-cm layers do (section 4d) is a clear indication that soil layer modifications are at times compensating for other inadequate model parameters. For example, soil hydraulic properties are specified based on lookup tables that do not necessarily reflect the scale of LSM or SMAP pixels (Hogue et al. 2006; Reynolds et al. 2000). These properties determine the ceiling and floor (porosity and wilting point) that confines the modeled or retrieved soil moisture. Any mismatch or unrealistic soil type information can therefore introduce model biases like those seen at some of the sites presented above (Xia et al. 2015; Gutmann and Small 2005).

The findings of this paper should be taken more as an indication of the importance of reconciling biases and ancillary data across satellite, LSMs, and in situ datasets than as an endorsement to utilize thinner model discretizations in Noah and Noah-MP. If the reader wishes to use layering schemes similar to those shown here, he or she must understand that model layer thicknesses may (as in Noah-MP) or may not (as in Noah) also be included as parameters in flux calculations that will affect the system more than the changes otherwise would alone. Future work should focus on improved calibration of LSMs using observations (in situ and/or satellite) so that bias issues in LSMs can be teased out separately from those in RTMs. Further examination of the role of soil layers in the model should be made in conjunction with revised parameters to investigate if positive improvements from calibration and layering adjustments can be made simultaneously.

Acknowledgments. This work has been funded by NASA ROSES NNH15ZDA001N-SUSMAP. The authors thank three anonymous reviewers for their helpful contributions. The authors declare no conflicts of interest.

REFERENCES

Ahuja, L. R., L. Ma, and T. R. Green, 2010: Effective soil properties of heterogeneous areas for modeling infiltration and redistribution. *Soil. Sci. Soc. Amer. J.*, **74**, 1469–1482, https://doi.org/10.2136/sssaj2010.0073.

Anagnostou, E. N., A. J. Negri, and R. F. Adler, 1999: Statistical adjustment of satellite microwave monthly rainfall estimates over Amazonia. *J. Appl. Meteor.*, **38**, 1590–1598, https://doi.org/10.1175/1520-0450(1999)038<1590:SAOSMM>2.0.CO;2.

Arsenault, K. R., and Coauthors, 2018a: The Land Surface Data Toolkit (LDT v7.2) – A data fusion environment for land data assimilation systems. *Geosci. Model Dev.*, **11**, 3605–3621, https://doi.org/10.5194/gmd-11-3605-2018.

——, G. S. Nearing, S. Wang, S. Yatheendradas, and C. D. Peters-Lidard, 2018b: Parameter sensitivity of the Noah-MP land surface model with dynamic vegetation. *J. Hydrometeor.*, **19**, 815–830, https://doi.org/10.1175/jhm-d-17-0205.1.

Atlas, D., D. Rosenfeld, and D. B. Wolff, 1990: Climatologically tuned reflectivity-rain rate relations and links to area-time integrals. *J. Appl. Meteor.*, **29**, 1120–1135, https://doi.org/10.1175/1520-0450(1990)029<1120:CTRRRR>2.0.CO;2.

Babaeian, E., M. Sadeghi, S. B. Jones, C. Montzka, H. Vereecken, and M. Tuller, 2019: Ground, proximal, and satellite remote sensing of soil moisture. *Rev. Geophys.*, **57**, 530–616, https://doi.org/10.1029/2018RG000618.

Ball, J. T., I. E. Woodrow, and J. A. Berry, 1987: A model predicting stomatal conductance and its contribution to the control of photosynthesis under different environmental conditions. *Progress in Photosynthesis Research*, Springer, 221–224.

Brunke, M. A., and Coauthors, 2016: Implementing and evaluating variable soil thickness in the Community Land Model, version 4.5 (CLM4.5). *J. Climate*, **29**, 3441–3461, https://doi.org/10.1175/JCLI-D-15-0307.1.

Brutsaert, W., 1982: *Evaporation into the Atmosphere*. Springer, 302 pp.

Chakravarti, I., R. Laha, and J. Roy, 1967: *Handbook of Methods of Applied Statistics*. John Wiley and Sons, 392–394 pp.

Chan, S. K., and Coauthors, 2016: Assessment of the SMAP passive soil moisture product. *IEEE Trans. Geosci. Remote Sens.*, **54**, 4994–5007, https://doi.org/10.1109/TGRS.2016.2561938.

——, and Coauthors, 2018: Development and assessment of the SMAP enhanced passive soil moisture product. *Remote Sens. Environ.*, **204**, 931–941, https://doi.org/10.1016/j.rse.2017.08.025.

Chaubell, M. J., and Coauthors, 2020: Improved SMAP dual-channel algorithm for the retrieval of soil moisture. *IEEE Trans. Geosci. Remote Sens.*, **58**, 3894–3905, https://doi.org/10.1109/TGRS.2019.2959239.

Chen, F., and J. Dudhia, 2001: Coupling an advanced land surface-hydrology model with the Penn State–NCAR MM5 modeling system. Part I: Model implementation and sensitivity. *Mon. Wea. Rev.*, **129**, 569–585, https://doi.org/10.1175/1520-0493(2001)129<0569:CAALSH>2.0.CO;2.

——, and Coauthors, 1996: Modeling of land surface evaporation by four schemes and comparison with FIFE observations. *J. Geophys. Res.*, **101**, 7251–7268, https://doi.org/10.1029/95JD02165.

Choudhury, B. J., T. J. Schmugge, A. Chang, and R. W. Newton, 1979: Effect of surface roughness on the microwave emission from soils. *J. Geophys. Res.*, **84**, 5699, https://doi.org/10.1029/JC084iC09p05699.

Colliander, A., and Coauthors, 2017a: Validation of SMAP surface soil moisture products with core validation sites. *Remote Sens. Environ.*, **191**, 215–231, https://doi.org/10.1016/j.rse.2017.01.021.

——, H. Al Jassar, W. Dorigo, J. Martinez-Fernandez, C. Montzka, and M. Seyfried, 2017b: SMAP/In situ core validation site land surface parameters match-up data, version 1. NASA NSIDC, accessed 30 October 2018, https://doi.org/10.5067/DXAVIXLY18KM.

Crow, W. T., R. D. Koster, R. H. Reichle, and H. O. Sharif, 2005: Relevance of time-varying and time-invariant retrieval error sources on the utility of spaceborne soil moisture products. *Geophys. Res. Lett.*, **32**, L24405, https://doi.org/10.1029/2005GL024889.

——, F. Chen, R. H. Reichle, and Y. Xia, 2019: Diagnosing bias in modeled soil moisture/runoff coefficient correlation using the

SMAP level 4 soil moisture product. *Water Resour. Res.*, **55**, 7010–7026, https://doi.org/10.1029/2019WR025245.

De Lannoy, G. J. M., and R. H. Reichle, 2016a: Assimilation of SMOS brightness temperatures or soil moisture retrievals into a land surface model. *Hydrol. Earth Syst. Sci.*, **20**, 4895–4911, https://doi.org/10.5194/hess-20-4895-2016.

——, and ——, 2016b: Global assimilation of multiangle and multipolarization SMOS brightness temperature observations into the GEOS-5 catchment land surface model for soil moisture estimation. *J. Hydrometeor.*, **17**, 669–691, https://doi.org/10.1175/JHM-D-15-0037.1.

——, ——, J. Peng, Y. Kerr, R. Castro, E. J. Kim, and Q. Liu, 2015: Converting between SMOS and SMAP level-1 brightness temperature observations over nonfrozen land. *IEEE Geosci. Remote Sens. Lett.*, **12**, 1908–1912, https://doi.org/10.1109/LGRS.2015.2437612.

Drusch, M., T. Holmes, P. de Rosnay, and G. Balsamo, 2009: Comparing ERA-40-based L-band brightness temperatures with skylab observations: A calibration/validation study using the community microwave emission model. *J. Hydrometeor.*, **10**, 213–226, https://doi.org/10.1175/2008JHM964.1.

Ek, M. B., K. E. Mitchell, Y. Lin, E. Rogers, P. Grunmann, V. Koren, G. Gayno, and J. D. Tarpley, 2003: Implementation of Noah land surface model advances in the National Centers for Environmental Prediction operational mesoscale Eta model. *J. Geophys. Res.*, **108**, 8851, https://doi.org/10.1029/2002JD003296.

Entekhabi, D., and Coauthors, 2010: The Soil Moisture Active Passive (SMAP) mission. *Proc. IEEE*, **98**, 704–716, https://doi.org/10.1109/JPROC.2010.2043918.

——, and Coauthors, 2014: SMAP Handbook Soil Moisture Active Passive, Mapping Soil Moisture Freeze/Thaw from Space. 182 pp., https://smap.jpl.nasa.gov/system/internal_resources/details/original/178_SMAP_Handbook_FINAL_1_JULY_2014_Web.pdf.

Escorihuela, M. J., A. Chanzy, J. P. Wigneron, and Y. H. Kerr, 2010: Effective soil moisture sampling depth of L-band radiometry: A case study. *Remote Sens. Environ.*, **114**, 995–1001, https://doi.org/10.1016/j.rse.2009.12.011.

Felfelani, F., Y. Pokhrel, K. Guan, and D. M. Lawrence, 2018: Utilizing SMAP soil moisture data to constrain irrigation in the community land model. *Geophys. Res. Lett.*, **45**, 12 892–12 902, https://doi.org/10.1029/2018GL080870.

Gutmann, E. D., and E. E. Small, 2005: The effect of soil hydraulic properties vs. soil texture in land surface models. *Geophys. Res. Lett.*, **32**, L02402, https://doi.org/10.1029/2004GL021843.

——, and ——, 2007: A comparison of land surface model soil hydraulic properties estimated by inverse modeling and pedotransfer functions. *Water Resour. Res.*, **43**, W05418, https://doi.org/10.1029/2006WR005135.

——, and ——, 2010: A method for the determination of the hydraulic properties of soil from MODIS surface temperature for use in land-surface models. *Water Resour. Res.*, **46**, W06520, https://doi.org/10.1029/2009WR008203.

Hansen, M., R. DeFries, J. R. G. Townshend, and R. Sohlberg, 2000: Global land cover classification at 1 km spatial resolution using a classification tree approach. *Int. J. Remote Sens.*, **21**, 1331–1364, https://doi.org/10.1080/014311600210209.

Hogue, T. S., L. A. Bastidas, H. V. Gupta, and S. Sorooshian, 2006: Evaluating model performance and parameter behavior for varying levels of land surface model complexity. *Water Resour. Res.*, **42**, W08430, https://doi.org/10.1029/2005WR004440.

Holmes, T. R. H., M. Drusch, J.-P. Wigneron, and R. A. M. de Jeu, 2008: A global simulation of microwave emission: Error structures based on output from ECMWF's operational integrated forecast system. *IEEE Trans. Geosci. Remote Sens.*, **46**, 846–856, https://doi.org/10.1109/TGRS.2007.914798.

Kumar, S. V., P. A. Dirmeyer, C. D. Peters-Lidard, R. Bindlish, and J. Bolten, 2018: Information theoretic evaluation of satellite soil moisture retrievals. *Remote Sens. Environ.*, **204**, 392–400, https://doi.org/10.1016/j.rse.2017.10.016.

Jackson, T. J., and T. J. Schmugge, 1989: Passive microwave remote sensing system for soil moisture: Some supporting research. *IEEE Trans. Geosci. Remote Sens.*, **27**, 225–235, https://doi.org/10.1109/36.20301.

——, and ——, 1991: Vegetation effects on the microwave emission of soils. *Remote Sens. Environ.*, **36**, 203–212, https://doi.org/10.1016/0034-4257(91)90057-D.

——, ——, and J. R. Wang, 1982: Passive microwave sensing of soil moisture under vegetation canopies. *Water Resour. Res.*, **18**, 1137–1142, https://doi.org/10.1029/WR018i004p01137.

——, and Coauthors, 2012: Validation of Soil Moisture and Ocean Salinity (SMOS) soil moisture over watershed networks in the U.S. *IEEE Trans. Geosci. Remote Sens.*, **50**, 1530–1543, https://doi.org/10.1109/TGRS.2011.2168533.

Jaeger, E. B., and S. I. Seneviratne, 2011: Impact of soil moisture–atmosphere coupling on European climate extremes and trends in a regional climate model. *Climate Dyn.*, **36**, 1919–1939, https://doi.org/10.1007/s00382-010-0780-8.

Jordan, R., 1991: A one-dimensional temperature model for a snow cover: Technical documentation for SNTERERM.89. Special Rep. 91-16, Cold Region Research and Engineers Laboratory, U.S. Army Corps of Engineers, Hanover, NH, 61 pp.

Kerr, Y. H., and Coauthors, 2010: The SMOS mission: New tool for monitoring key elements ofthe global water cycle. *Proc. IEEE*, **98**, 666–687, https://doi.org/10.1109/JPROC.2010.2043032.

Koster, R. D., and P. C. D. Milly, 1997: The interplay between transpiration and runoff formulations in land surface schemes used with atmospheric models. *J. Climate*, **10**, 1578–1591, https://doi.org/10.1175/1520-0442(1997)010<1578:TIBTAR>2.0.CO;2.

——, Z. Guo, R. Yang, P. Dirmeyer, K. Mitchell, and M. J. Puma, 2009: On the nature of soil moisture in land surface models. *J. Climate*, **22**, 4322–4335, https://doi.org/10.1175/2009JCLI2832.1.

Kumar, S. V., and Coauthors, 2006: Land information system: An interoperable framework for high resolution land surface modeling. *Environ. Modell. Software*, **21**, 1402–1415, https://doi.org/10.1016/j.envsoft.2005.07.004.

——, C. D. Peters-Lidard, J. Santanello, K. Harrison, Y. Liu, and M. Shaw, 2012a: Land surface Verification Toolkit (LVT) – A generalized framework for land surface model evaluation. *Geosci. Model Dev.*, **5**, 869–886, https://doi.org/10.5194/gmd-5-869-2012.

——, R. H. Reichle, K. W. Harrison, C. D. Peters-Lidard, S. Yatheendradas, and J. A. Santanello, 2012b: A comparison of methods for a priori bias correction in soil moisture data assimilation. *Water Resour. Res.*, **48**, W03515, https://doi.org/10.1029/2010WR010261.

——, and Coauthors, 2014a: Assimilation of remotely sensed soil moisture and snow depth retrievals for drought estimation. *J. Hydrometeor.*, **15**, 2446–2469, https://doi.org/10.1175/JHM-D-13-0132.1.

——, K. W. Harrison, C. D. Peters-Lidard, J. A. Santanello, and D. Kirschbaum, 2014b: Assessing the impact of L-band

observations on drought and flood risk estimation: A decision-theoretic approach in an OSSE environment. *J. Hydrometeor.*, **15**, 2140–2156, https://doi.org/10.1175/JHM-D-13-0204.1.

——, C. D. Peters-Lidard, J. A. Santanello, R. H. Reichle, C. S. Draper, R. D. Koster, G. Nearing, and M. F. Jasinski, 2015: Evaluating the utility of satellite soil moisture retrievals over irrigated areas and the ability of land data assimilation methods to correct for unmodeled processes. *Hydrol. Earth Syst. Sci.*, **19**, 4463–4478, https://doi.org/10.5194/hess-19-4463-2015.

Kurc, S. A., and E. E. Small, 2004: Dynamics of evapotranspiration in semiarid grassland and shrubland ecosystems during the summer monsoon season, central New Mexico. *Water Resour. Res.*, **40**, W09305, https://doi.org/10.1029/2004WR003068.

Lahoz, W. A., and G. J. M. De Lannoy, 2014: Closing the gaps in our knowledge of the hydrological cycle over land: Conceptual problems. *Surv. Geophys.*, **35**, 623–660, https://doi.org/10.1007/s10712-013-9221-7.

Lawston, P. M., J. A. Santanello, T. E. Franz, and M. Rodell, 2017a: Assessment of irrigation physics in a land surface modeling framework using non-traditional and human-practice datasets. *Hydrol. Earth Syst. Sci.*, **21**, 2953–2966, https://doi.org/10.5194/hess-21-2953-2017.

——, ——, and S. V. Kumar, 2017b: Irrigation signals detected from SMAP soil moisture retrievals. *Geophys. Res. Lett.*, **44**, 11 860–11 867, https://doi.org/10.1002/2017GL075733.

Lehmann, P., O. Merlin, P. Gentine, and D. Or, 2018: Soil texture effects on surface resistance to bare-soil evaporation. *Geophys. Res. Lett.*, **45**, 10 398–10 405, https://doi.org/10.1029/2018GL078803.

Liu, P.-W., R. D. De Roo, A. W. England, and J. Judge, 2013: Impact of moisture distribution within the sensing depth on L- and C-band emission in sandy soils. *IEEE J. Sel. Top. Appl. Earth Obs. Remote Sens.*, **6**, 887–899, https://doi.org/10.1109/JSTARS.2012.2213239.

Miller, D. A., and R. A. White, 1998: A conterminous United States multilayer soil characteristics dataset for regional climate and hydrology modeling. *Earth Interact.*, **2**, 1–26, https://doi.org/10.1175/1087-3562(1998)002<0001:ACUSMS>2.3.CO;2.

Mironov, V. L., L. G. Kosolapova, and S. V. Fomin, 2009: Physically and mineralogically based spectroscopic dielectric model for moist soils. *IEEE Trans. Geosci. Remote Sens.*, **47**, 2059–2070, https://doi.org/10.1109/TGRS.2008.2011631.

Niu, G.-Y., and Z.-L. Yang, 2004: Effects of vegetation canopy processes on snow surface energy and mass balances. *J. Geophys. Res.*, **109**, D23111, https://doi.org/10.1029/2004JD004884.

——, and ——, 2006: Effects of frozen soil on snowmelt runoff and soil water storage at a continental scale. *J. Hydrometeor.*, **7**, 937–952, https://doi.org/10.1175/JHM538.1.

——, ——, R. E. Dickinson, L. E. Gulden, and H. Su, 2007: Development of a simple groundwater model for use in climate models and evaluation with Gravity Recovery and Climate Experiment data. *J. Geophys. Res.*, **112**, D07103, https://doi.org/10.1029/2006JD007522.

——, and Coauthors, 2011: The community Noah land surface model with multiparameterization options (Noah-MP): 1. Model description and evaluation with local-scale measurements. *J. Geophys. Res.*, **116**, D12109, https://doi.org/10.1029/2010JD015139.

Njoku, E. G., and J.-A. Kong, 1977: Theory for passive microwave remote sensing of near-surface soil moisture. *J. Geophys. Res.*, **82**, 3108–3118, https://doi.org/10.1029/JB082i020p03108.

Ozdogan, M., M. Rodell, H. K. Beaudoing, and D. L. Toll, 2010: Simulating the effects of irrigation over the United States in a land surface model based on satellite-derived agricultural data. *J. Hydrometeor.*, **11**, 171–184, https://doi.org/10.1175/2009JHM1116.1.

O'Neill, P., R. Bindlish, S. Chan, E. G. Njoku, and T. J. Jackson, 2018: Algorithm theoretical basis document level 2 & 3 soil moisture (passive) data products, revision D. Jet Propulsion Laboratory Rep. JPL D-66480, 82 pp., https://smap.jpl.nasa.gov/system/internal_resources/details/original/484_L2_SM_P_ATBD_rev_D_Jun2018.pdf.

Peters-Lidard, C. D., and Coauthors, 2007: High-performance earth system modeling with NASA/GSFC's land information system. *Innov. Syst. Softw. Eng.*, **3**, 157–165, https://doi.org/10.1007/s11334-007-0028-x.

Rains, D., X. Han, H. Lievens, C. Montzka, and N. E. C. Verhoest, 2017: SMOS brightness temperature assimilation into the Community Land Model. *Hydrol. Earth Syst. Sci.*, **21**, 5929–5951, https://doi.org/10.5194/hess-21-5929-2017.

Reichle, R. H., and R. D. Koster, 2004: Bias reduction in short records of satellite soil moisture. *Geophys. Res. Lett.*, **31**, L19501, https://doi.org/10.1029/2004GL020938.

——, D. B. McLaughlin, and D. Entekhabi, 2002: Hydrologic data assimilation with the ensemble Kalman filter. *Mon. Wea. Rev.*, **130**, 103–114, https://doi.org/10.1175/1520-0493(2002)130<0103:HDAWTE>2.0.CO;2.

Reynolds, C. A., T. J. Jackson, and W. J. Rawls, 2000: Estimating soil water-holding capacities by linking the Food and Agriculture Organization Soil map of the world with global pedon databases and continuous pedotransfer functions. *Water Resour. Res.*, **36**, 3653–3662, https://doi.org/10.1029/2000WR900130.

Rondinelli, W. J., B. K. Hornbuckle, J. C. Patton, M. H. Cosh, V. A. Walker, B. D. Carr, and S. D. Logsdon, 2015: Different rates of soil drying after rainfall are observed by the SMOS satellite and the South Fork in situ soil moisture network. *J. Hydrometeor.*, **16**, 889–903, https://doi.org/10.1175/JHM-D-14-0137.1.

Sakaguchi, K., and X. Zeng, 2009: Effects of soil wetness, plant litter, and under-canopy atmospheric stability on ground evaporation in the Community Land Model (CLM3.5). *J. Geophys. Res.*, **114**, D01107, https://doi.org/10.1029/2008JD010834.

Santanello, J. A., and T. N. Carlson, 2001: Mesoscale simulation of rapid soil drying and its implications for predicting daytime temperature. *J. Hydrometeor.*, **2**, 71–88, https://doi.org/10.1175/1525-7541(2001)002<0071:MSORSD>2.0.CO;2.

——, P. Lawston, S. Kumar, and E. Dennis, 2019: Understanding the impacts of soil moisture initial conditions on NWP in the context of land–atmosphere coupling. *J. Hydrometeor.*, **20**, 793–819, https://doi.org/10.1175/JHM-D-18-0186.1.

Shellito, P. J., and Coauthors, 2016a: SMAP soil moisture drying more rapid than observed in situ following rainfall events. *Geophys. Res. Lett.*, **43**, 8068–8075, https://doi.org/10.1002/2016GL069946.

——, E. E. Small, and M. H. Cosh, 2016b: Calibration of Noah soil hydraulic property parameters using surface soil moisture from SMOS and basinwide in situ observations. *J. Hydrometeor.*, **17**, 2275–2292, https://doi.org/10.1175/JHM-D-15-0153.1.

Ulaby, F. T., R. K. Moore, and A. K. Fung, 1981: *Microwave Remote Sensing: Active and Passive*. Vol. 3, *Theory to Applications*. Artech House Publishers, 2162 pp.

Van Looy, K., and Coauthors, 2017: Pedotransfer functions in earth system science: Challenges and perspectives. *Rev. Geophys.*, **55**, 1199–1256, https://doi.org/10.1002/2017RG000581.

Verseghy, D. L., 1991: CLASS-A Canadian land surface scheme for GCMS. I. Soil model. *Int. J. Climatol.*, **11**, 111–133, https://doi.org/10.1002/joc.3370110202.

Wang, J. R., 1983: Passive microwave sensing of soil moisture content: The effects of soil bulk density and surface roughness. *Remote Sens. Environ.*, **13**, 329–344, https://doi.org/10.1016/0034-4257(83)90034-2.

Wegmüller, U., and C. Mätzler, 1999: Rough bare soil reflectivity model. *IEEE Trans. Geosci. Remote Sens.*, **37**, 1391–1395, https://doi.org/10.1109/36.763303.

Wood, A. W., 2002: Long-range experimental hydrologic forecasting for the eastern United States. *J. Geophys. Res.*, **107**, 4429, https://doi.org/10.1029/2001JD000659.

Xia, Y., and Coauthors, 2012: Continental-scale water and energy flux analysis and validation for the North American Land Data Assimilation System project phase 2 (NLDAS-2): 1. Intercomparison and application of model products. *J. Geophys. Res.*, **117**, D03109, https://doi.org/10.1029/2011JD016051.

——, M. B. Ek, Y. Wu, T. Ford, and S. M. Quiring, 2015: Comparison of NLDAS-2 simulated and NASMD observed daily soil moisture. Part II: Impact of soil texture classification and vegetation type mismatches. *J. Hydrometeor.*, **16**, 1981–2000, https://doi.org/10.1175/JHM-D-14-0097.1.

Yang, Z.-L., and Coauthors, 2011: The community Noah land surface model with multiparameterization options (Noah-MP): 2. Evaluation over global river basins. *J. Geophys. Res.*, **116**, D12110, https://doi.org/10.1029/2010JD015140.

Zhang, X., J. Qiu, G. Leng, Y. Yang, Q. Gao, Y. Fan, and J. Luo, 2018: The potential utility of satellite soil moisture retrievals for detecting irrigation patterns in China. *Water*, **10**, 1–505, https://doi.org/10.3390/w10111505.